PHILOSOPHICAL TRANSACTIONS OF THE ROYAL SOCIETY A MATHEMATICAL, PHYSICAL & ENGINEERING SCIENCES

The Rydberg spectrum of ArH and KrH: calculation by *R*–matrix and generalized quantum defect theory

Ch. Jungen, A. L. Roche and M. Arif

Phil. Trans. R. Soc. Lond. A 1997 **355**, 1481-1506
doi: 10.1098/rsta.1997.0072

The Rydberg spectrum of ArH and KrH: calculation by *R*-matrix and generalized quantum defect theory

By Ch. Jungen[1], A. L. Roche[2] and M. Arif[1]†

[1]*Laboratoire Aimé Cotton du CNRS, Université de Paris-Sud, 91405 Orsay, France*

[2]*Laboratoire de Photophysique Moléculaire du CNRS, Université de Paris-Sud, 91405 Orsay, France*

The generalized ligand field approach developed recently by Arif and others for the description of the electronic structures of the alkaline earth halides is used to calculate the electronic spectrum of ArH and of KrH from the ground state up near the ionization limit. The ion core is represented as a closed-shell protonated rare gas atom from which the lone electron is scattered. The resulting level energies (effective principal quantum numbers) are in good agreement with the available experimental data and constitute the first global theoretical calculation of the electronic spectra of ArH and KrH. Polarization of the rare gas atom by the ligand proton is shown to be significant.

1. Introduction

The rare gas monohydrides are all known to have unstable ground states, but they all possess extended systems of stable excited states which are all Rydberg states. They are therefore commonly referred to as 'Rydberg molecules' and as such belong to a particular class of 'excimer' systems (Herzberg 1987). The experimentally observed Rydberg series of the rare gas hydrides have progressively emerged in recent years from numerous studies of Rydberg–Rydberg emission bands in the visible and infrared spectral regions, studied by Fourier transform spectroscopy (Dabrowski *et al.* 1996; Dabrowski *et al.* 1997*a*, *b*; Dabrowski & Sadovskii 1994 and references therein).

The question then arises, as to where the Rydberg electron comes from: is it excited from the hydrogen atom or from the rare gas atom? In other terms, are the rare gas hydrides better described as $(\mathrm{Rg}\cdot\mathrm{H}^+)\mathrm{e}^-$ or as $(\mathrm{Rg}^+\cdot\mathrm{H})\mathrm{e}^-$? At the crudest level of approximation we can answer this question by comparing the ionization energies of the various rare gas atoms with that of a hydrogen atom. This is done in table 1 and figure 1 (dotted lines) where it can be seen that HeH, NeH and ArH can probably be regarded as Rydberg molecules built on a protonated rare gas atom core $(\mathrm{Rg}\cdot\mathrm{H}^+)$, whereas this description appears as doubtful for KrH and frankly incorrect for XeH.

We can improve this picture by taking account of polarization in the molecular

† Present address: Département de Physique, Université de Tunis, Tunis 1060, Tunisia.

Phil. Trans. R. Soc. Lond. A (1997) **355**, 1481–1506
Printed in Great Britain

Table 1. *Ionization energies and dipole polarizabilities of rare gas atoms*

	IP [a]	α_d [b]	R_e^+ [c]	$E(\mathrm{Rg}^+ \cdot \mathrm{H})$ [d]	$E(\mathrm{Rg} \cdot \mathrm{H}^+)$ [e]	ΔE [f]	Q_1 [g]	$\alpha_d^{(\mathrm{eff})}$ [h]
H	0.999	4.5						
He	1.807	1.32	1.48	0.87	0.72	0.15	0.24	1.10
Ne	1.585	2.67	1.88	1.22	0.79	0.43	0.29	2.32
Ar	1.158	10.76	2.43	1.03	0.68	0.35	−0.33	9.14
Kr	1.029	16.78	2.68	0.94	0.67	0.27	−0.57	13.70
Xe	0.892	27.32	3.04	0.84	0.68	0.16	−0.89	22.25

[a]Ionization energy in Rydbergs (Moore 1971).
[b]Atomic dipole polarizability (a_0^3, Cuthbertson & Cuthbertson 1932).
[c]Equilibrium bond distance of $(\mathrm{RgH})^+$ (a_0, Rosmus & Reinsch 1980; Rosmus 1979; Klein & Rosmus 1984).
[d]Rydbergs, equation (1.1 *b*).
[e]Rydbergs, equation (1.1 *a*).
[f]Rydbergs, $E(\mathrm{Rg}^+ \cdot \mathrm{H}) - E(\mathrm{Rg} \cdot \mathrm{H}^+)$.
[g]*Ab initio* dipole moment of $(\mathrm{RgH})^+$ with respect to the molecular midpoint (a_0, Klein & Rosmus 1984).
[h]'Effective' atomic dipole polarizability (a_0^3), deduced by inverting equation (2.10 *b*) with the *ab initio* values for R and Q_1 from columns 4 and 8, respectively.

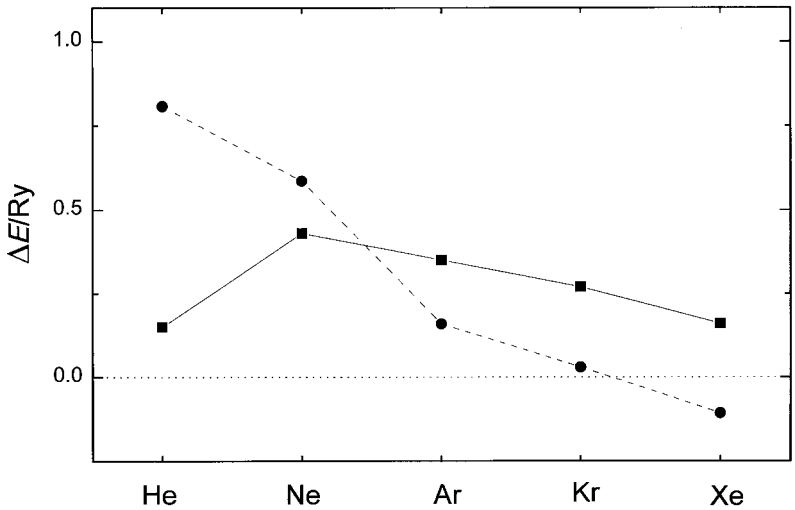

Figure 1. Stability of the protonated rare gas configuration for various rare gas hydride ions. The dots/broken lines correspond to the differences of ionization potentials IP(Rg) − IP(H). The squares/full lines correspond to equation (1.1) which also accounts for the polarization of the rare gas atom by the proton. Positive values ΔE indicate that the protonated rare gas structure is favoured.

ion core. The energy of a protonated rare gas atom is thus approximated by

$$E(\mathrm{Rg} \cdot \mathrm{H}^+) = (\mathrm{IP})_{\mathrm{H}} - (\alpha_{\mathrm{Rg}}/R^4), \qquad (1.1\,a)$$

where α_{Rg} is the dipole polarizability of the free rare gas atom in units of a_0^3, R is the equilibrium internuclear distance of the ion core in units of a_0 and the energy is in Rydberg units. The inverse description yields

$$E(\mathrm{Rg}^+ \cdot \mathrm{H}) = (\mathrm{IP})_{\mathrm{Rg}} - (\alpha_{\mathrm{H}}/R^4). \qquad (1.1\,b)$$

Using the known values for α and R listed in table 1 we plot in figure 1 (full lines) the difference $\Delta E = E(\mathrm{Rg}^+ \cdot \mathrm{H}) - E(\mathrm{Rg} \cdot \mathrm{H}^+)$, which tells us how much more stable the protonated rare gas atom configuration is expected to be compared to the configuration $\mathrm{Rg}^+ \cdot \mathrm{H}$. While, of course, it still gives only a rough account of the reality, figure 1 does indicate that all rare gas hydride Rydberg states, from HeH through to XeH, should near equilibrium correspond to a protonated rare gas atom core with an associated electron. The reason is that the heavier the rare gas atom, the larger is its polarizability, in such a way that the configuration $\mathrm{Rg} \cdot \mathrm{H}^+$ is stable in spite of the reduced value of $(\mathrm{IP})_{\mathrm{Rg}}$. Further evidence for the qualitative correctness of this picture comes from consideration of the core dipole moments which are known quite precisely by *ab initio* calculations, as will be discussed in § 3 *b*.

In this paper we present calculations of the Rydberg series of ArH and KrH which are based on the assumption that these can be described as $(\mathrm{Rg} \cdot \mathrm{H}^+)\mathrm{e}^-$. These calculations are complementary to quantum chemical calculations for the same systems (Petsalakis & Theodorakopoulos 1994). Here we give a multichannel description of the *full* Rydberg spectrum of these molecules up near the ionization energy (and, in principle, of the inelastic electron-core scattering matrices in the electronic continuum beyond), whereas the available quantum chemical calculations are limited to the lowest few excited states which are calculated individually. Our effective one-electron approach, on the other hand, while providing a global description of the rare gas hydrides near equilibrium, is unable to account for the dissociation behaviour which involves strong mixing between the $(\mathrm{Rg} \cdot \mathrm{H}^+)\mathrm{e}^-$ and $(\mathrm{Rg}^+ \cdot \mathrm{H})\mathrm{e}^-$ configurations.

2. Theory

Our calculations are based on R-matrix theory combined with generalized quantum defect theory and constitute a new application of the generalized ligand field approach which we developed recently for the alkaline earth halides (in particular, CaF and BaF) (Arif *et al.* 1997, subsequently referred to as AJR). These molecules were described successfully as $(\mathrm{M}^{++} \cdot \mathrm{X}^-)\mathrm{e}^-$, i.e. 'Rydberg' molecules possessing a double closed-shell core with charges $Z_1 = +2$ and $Z_2 = -1$ plus an associated electron. In the present work we take over the formalism of AJR without change by simply setting $Z_1 = 0$ and $Z_2 = +1$ in the relevant expressions. A detailed account of the theory has been given in AJR. In the following we give an abbreviated survey of the method.

The method of calculation involves separate treatments adapted to various regions of space. Figure 2 illustrates the partitioning of space which we use.

(*a*) *Atomic reaction zone I*

The atomic zone I corresponds to the rare gas atom and is characterized by correlated motions of the electrons of the rare gas and the additional molecular electron. We do not attempt here to describe this region in detail, but instead represent its net effect on the motion of the molecular electron by a boundary condition applied to each partial wave l at the atom surface. Thus we have

$$-\frac{\partial(r_1\psi_l^{\mathrm{I}})/\partial r_1}{(r_1\psi_l^{\mathrm{I}})} = -\frac{\partial(r_1\psi_l^{\mathrm{II}})/\partial r_1}{(r_1\psi_l^{\mathrm{II}})} = b_l(r_1) \quad (r_1 = r_{1\mathrm{a}}), \tag{2.1}$$

where r_1 is the electron distance from the rare gas atom nucleus and $r_{1\mathrm{a}}$ the atomic radius. $\psi_l^{\mathrm{I}}(\epsilon, r_1, \theta_1, \phi_1)$ is the wavefunction of the lone electron l emerging from closed-

shell rare gas atom, while ψ_l^{II} is the corresponding term in the partial wave expansion valid in the molecular zone II surrounding the atom.

The quantities $b_l(r_{1a})$ characterize the electron–atom interaction and are equivalent to the elastic electron–atom scattering phase-shifts which are well known as functions of the electron energy both from experiment and *ab initio* theory. We shall see below that an efficient way of evaluating the set of boundary conditions b_l involves the determination of a set of pseudo-potentials $V_l^{(\mathrm{core})}(r_1)$ which adequately represent the energy-dependent partial wave asymptotic phase shifts, followed by numerical integration of the one-electron Schrödinger equation from $r_1 = 0$ out to $r_1 = r_{1a}$. The logarithmic derivative of each partial wave ψ_l is thus obtained at this point.

(*b*) *Molecular reaction zone II*

The zone II in figure 2 is the molecular or 'reaction' zone which is intermediate between the short-range atomic region and the asymptotic Coulombic region. Here we approximate the electron wavefunction by that of the single molecular electron. Its motion, however, is non-separable owing to the presence of the additional molecular core proton. The electron potential energy is represented by the expression

$$\begin{aligned} V_l(\boldsymbol{r}_1, \boldsymbol{r}_2, R) = &- \left[\frac{2Z_1}{r_1} + \frac{2Z_2}{r_2}\right] \\ &+ \left[- \alpha_1 f_1^2 \frac{1}{r_1^4} + \alpha_1 f_1 \frac{2Z_2 \cos\theta_1}{r_1^2 R^2} - \alpha_2 f_2^2 \frac{1}{r_2^4} + \alpha_2 f_2 \frac{2Z_1 \cos\theta_2}{r_2^2 R^2}\right] \\ &- \frac{4\alpha_1 f_1 \alpha_2 f_2}{R^5}\left[\frac{Z_1 \cos\theta_1}{r_1^2} + \frac{Z_2 \cos\theta_2}{r_2^2}\right] \\ &+ \frac{2\alpha_1 f_1 \alpha_2 f_2}{R^3 r_1^2 r_2^2}[2\cos\theta_1 \cos\theta_2 + \sin\theta_1 \sin\theta_2] + V_l^{(\mathrm{core})}(r_1), \end{aligned} \tag{2.2}$$

with the following definitions: r_1 and r_2 are defined in figure 2. The polar angles θ_1 and θ_2 are defined such that $\theta_1 = \theta_2 = 0$ at the molecular midpoint. Z_1 and Z_2 are the electric charges carried by the two scattering centres and α_1 and α_2 are the corresponding dipole polarizabilities. As stated earlier, we take $Z_1 = 0$, $Z_2 = 1$ and $\alpha_2 = 0$ in the present application. f_1 and f_2 are the customary cut-off functions for the polarization potentials of the two centres defined as

$$f_1(r_1) = [1 - \mathrm{e}^{-(r_1/r_{1c})^6}]^{1/2}, \tag{2.3}$$

with r_{1c} the cut-off radius. Both r_{1c} in equation (2.3) and r_{1a} in equation (2.1) are measures for the rare gas atom radius and thus $r_{1c} \approx r_{1a}$. The two quantities are distinguished here only because of their different role in the formalism. The five terms of equation (2.2) correspond, in this order, to the following interactions: (a) the Coulomb interaction between Z_1, Z_2 and e^-; (b) the energy of the electric dipole induced on each centre by the electron and by the charge of the other centre; (c) the dipole–dipole interaction energy of each electron-induced dipole on one centre with the ion-induced dipole on the other centre; (d) the dipole–dipole interaction energy of the two electron-induced dipoles; and (e) an l-dependent rare gas atom correction potential which decreases exponentially outside the core (cf. § 3 *b*).

All the terms that are independent of the position of the electron (such as, for example, the dipole–dipole interaction energy between the dipoles induced on each

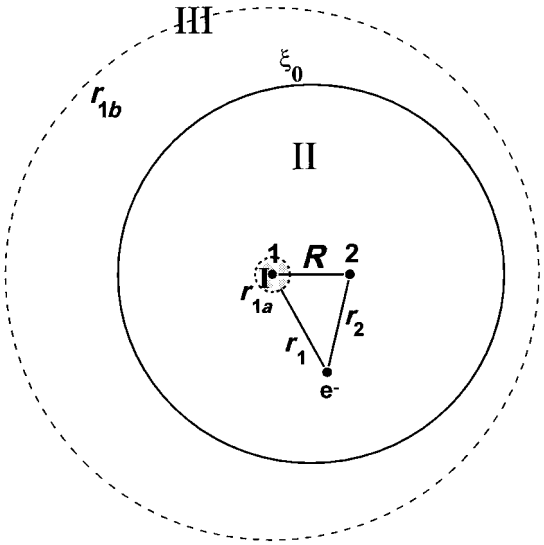

Figure 2. Schematic representation of an electron interacting with a protonated rare gas atom: 1, rare gas nucleus; 2, proton; I, atomic zone; II, molecular ('reaction') zone; III, asymptotic zone. The spheres $r = r_{1a}$, $r = r_{1b}$ and the ellipsoid $\xi = \xi_0$ are the boundaries used in the R matrix calculation (cf. the text).

centre by the other centre) are considered to be part of the energy of the molecular ion core and are thus omitted.

The non-separable motion of the molecular electron in the reaction zone II is treated by setting up a Hamiltonian matrix in terms of a set of basis functions. We chose a basis defined for $r_{1a} \leqslant r_1 \leqslant r_{1b}$ (see figure 2), where r_{1b} must be sufficiently large as we will discuss below. The basis consists of spherical free-particle eigenfunctions of the form

$$\psi_{ml}^{(\lambda)}(r_1,\theta_1,\phi) = Y_{l\lambda}(\theta_1,\phi)\frac{1}{r_1}[c_{ml}\sin(k_{ml}r_1) + d_{ml}\cos(k_{ml}r_1)], \quad (\epsilon_{ml}^{(\lambda)} = \tfrac{1}{2}k_{ml}^2 \geqslant 0),$$
$$\psi_{ml}^{(\lambda)}(r_1,\theta_1,\phi) = Y_{l\lambda}(\theta_1,\phi)\frac{1}{r_1}[c_{ml}\mathrm{e}^{\kappa_{ml}r_1} + d_{ml}\mathrm{e}^{-\kappa_{ml}r_1}], \quad (\epsilon_{ml}^{(\lambda)} = -\tfrac{1}{2}\kappa_{ml}^2 \leqslant 0). \quad (2.4)$$

The coefficients c_{ml} and d_{ml} are determined by imposition of specific boundary conditions at $r_1 = r_{1a}$ and $r_1 = r_{1b}$. At the inner edge of zone II we impose the set of conditions equation (2.1), whereas the condition imposed at the outer edge is arbitrary but fixed and will be specified in § 3 *d*. For a given set of conditions $b_l(r_{1a})$ and $b_l(r_{1b})$ we obtain a discrete set of energies $\epsilon_{ml}^{(\lambda)}$ $(m = 0, 1, \ldots)$ and orthonormalized eigenfunctions. Details are given in Appendix 1 of AJR. Figure 3 illustrates the lowest radial basis levels and functions with $l = 0$ such as used in a typical calculation.

In the next step a Hamiltonian matrix, diagonal in λ, is set up for each λ with elements given by the volume integrals

$$H_{ml,m'l'}^{(\lambda)}(R) = +\epsilon_{ml}^{(\lambda)}\delta_{ml,m'l'} + \int\int\int \psi_{ml}^{(\lambda)*}(r_1,\theta_1,\phi)\left[V_l(\boldsymbol{r}_1,\boldsymbol{r}_2,R) + \frac{l(l+1)}{r_1^2}\right]$$
$$\times\psi_{m'l'}^{(\lambda)}(r_1,\theta_1,\phi)r_1^2\sin\theta_1\,\mathrm{d}r_1\,\mathrm{d}\theta_1\,\mathrm{d}\phi. \quad (2.5)$$

Diagonalization of this matrix yields eigenvalues and eigenfunctions of the one-electron Hamiltonian valid in the range $r_{1a} \leqslant r_1 \leqslant r_{1b}$ which at $r_1 = r_{1a}$ reduce

to a superposition of atomic functions $\psi_l^{\mathrm{I}}(r_{1\mathrm{a}})$ as required by equation (2.1). These eigenenergies and eigenfunctions depend on the boundary condition $b(r_{1\mathrm{b}})$ imposed at the outer boundary $r_1 = r_{1\mathrm{b}}$. $b(r_{1\mathrm{b}})$ may then be varied iteratively and, each time an eigenvalue of $\boldsymbol{H}$ coincides with the desired total energy ϵ, an eigenvalue b of the boundary condition corresponding to that particular energy has been found. This is equivalent to the iterative eigenchannel R-matrix procedure of Fano & Lee (1973).

A more direct but otherwise equivalent method is the variational R-matrix scheme such as formulated by Greene (1983). Here one solves a generalized eigenvalue system which directly yields the set of eigenvalues b_β ($\beta = 1, 2, \ldots$) for the boundary condition on the outer sphere $r_1 = r_{1\mathrm{b}}$ and any preselected total energy ϵ. The matrices defining the generalized eigenvalue system are set up in terms of the Hamiltonian matrix of equation (2.5) plus angular overlap integrals between the basis functions of equation (2.4). Details are given in AJR.

The solution yields a set of coefficients $a_{ml,\beta}$ associated with each b_β value, which serve to construct the eigenfunctions valid in the reaction zone II in terms of the basis of equation (2.4):

$$\Psi_\beta^{\mathrm{II}} = \sum_{m,l} a_{ml,\beta}^{(\lambda)} \psi_{ml}^{(\lambda)}, \tag{2.6}$$

for each ϵ, R and λ.

(*c*) *Asymptotic zone III*

The next step of the treatment requires matching the solutions $\Psi_\beta^{\mathrm{II}(\lambda)}(\epsilon, R)$ to asymptotic separable channel functions. This procedure yields the desired reaction matrix, equivalent to the scattering matrix, which subsequently is used for bound state or scattering calculations.

At large electron distances the one-electron Hamiltonian corresponding to the potential equation (2.2) becomes separable either in spherical coordinates centred on the centre of mass of the molecule or in elliptic coordinates. We use the latter since they allow the long-range core dipole field to be taken into account exactly. As a result, we will find that the reaction zone II (radius $r_{1\mathrm{b}}$) can be taken to be relatively small and the convergence of the calculations is thus facilitated. Expressing V in terms of elliptic coordinates

$$\xi = \frac{r_1 + r_2}{R} \quad (1 \leqslant \xi \leqslant \infty), \quad \eta = \frac{r_1 - r_2}{R} \quad (-1 \leqslant \eta \leqslant +1), \quad \phi = \phi_1, \tag{2.7}$$

we find that for large r_1 and r_2 such that $\xi \gg 1 \geqslant \eta$,

$$V(\boldsymbol{r}_1, \boldsymbol{r}_2, R) \approx -\frac{4}{R(\xi^2 - \eta^2)} \left\{ \left[(Z_1 + Z_2) + \frac{4}{R^3 \xi^3} (\alpha_1 + \alpha_2) \right] \xi - (Z_1^{(\mathrm{eff})} - Z_2^{(\mathrm{eff})}) \eta \right\}, \tag{2.8}$$

with

$$Z_2^{(\mathrm{eff})} = Z_2 \left(1 - \frac{2\alpha_1}{R^3} - \frac{4\alpha_1 \alpha_2}{R^6} \right), \tag{2.9}$$

and where $Z_1^{(\mathrm{eff})}$ is defined accordingly.

Equation (2.8) is a variant of the familiar electrostatic potential created by two point charges. It contains an added radial polarization contribution and its angular dependence is also modified by polarization effects through the appearance of two *effective* charges $Z_i^{(\mathrm{eff})}$ which replace the usual integral charges Z_i. The charge difference in equation (2.8) is related to the core dipole moment Q_1 taken with respect

Table 2. *Pseudo-potential parameters for Ar^- and Kr^-*

	$Ar \cdot e^-$				$Kr \cdot e^-$			
	$l=0$	1	2	$\geqslant 3$	0	1	2	$\geqslant 3$
$a_1^{(l)}$	4.3312	4.2472	4.3463	4.3463	4.3248	4.2291	4.6754	4.6754
$b_1^{(l)}$	10.996	10.330	18.629	10.396	10.8930	10.3750	18.688	3.2451
$c_1^{(l)}$	1.4824	1.3981	2.0110	2.3454	1.4050	1.3710	1.6975	1.7617
$r_{1c}^{(l)}$	1.7178	1.8090	1.8161	1.8161	1.7344	1.8217	1.5571	1.5571

to the molecular midpoint,

$$Q_1 = \tfrac{1}{2}R(Z_2^{(\mathrm{eff})} - Z_1^{(\mathrm{eff})}), \tag{2.10 a}$$

or, for the diatomic rare gas hydrides,

$$Q_1 = \tfrac{1}{2}R\left(1 - \frac{2\alpha_1}{R^3}\right). \tag{2.10 b}$$

Equation (2.10 *b*) expresses the fact that the polarization of the rare gas atom by the nearby proton tends to reduce the molecular ion core dipole moment.

Numerical solution of the separable one-electron Schrödinger equation with the potential of equation (2.8) yields dipolar angular functions $\tilde{Y}_{\tilde{l}\lambda}(\eta,\phi)$ which are dipole distorted spherical harmonics. Radial regular and irregular functions $\tilde{f}_{\tilde{l}}(\epsilon,\xi)$ and $\tilde{g}_{\tilde{l}}(\epsilon,\xi)$ are evaluated as detailed in AJR.

With the asymptotic separable wavefunctions defined we next choose a value ξ_0 in order to match each solution $\Psi_\beta^{\mathrm{II}(\lambda)}$ obtained in zone II for a given λ to the asymptotic functions valid in region III. With ξ_0 large enough so that equation (2.8) holds we can use the following expansion:

$$\begin{aligned}\Psi_\beta^{\mathrm{II}}(\epsilon,\xi_0,\eta,\phi) &= \Psi_\beta^{\mathrm{III}}(\epsilon,\xi_0,\eta,\phi)\\ &\equiv \sum_{\tilde{l}} \tilde{Y}_{\tilde{l}\lambda}(\epsilon,\eta,\phi)\frac{1}{\sqrt{\xi_0^2-1}}[\tilde{f}_{\tilde{l}}(\epsilon,\xi_0)I_{\tilde{l}\beta}(\epsilon) - \tilde{g}_{\tilde{l}}(\epsilon,\xi_0)J_{\tilde{l}\beta}(\epsilon)].\end{aligned} \tag{2.11}$$

(For the sake of clarity the indices λ and R on Ψ, $\tilde{f}$, $\tilde{g}$, I and J are omitted here and later.) $\boldsymbol{I}$ and $\boldsymbol{J}$ are determined by the requirement that equation (2.11) and its derivative with respect to ξ be continuous at $\xi = \xi_0$. This is done by first expanding $\Psi_\beta^{\mathrm{II}}(\xi_0)$ and its derivative with respect to ξ in terms of the 'surface harmonics' $\tilde{Y}_{\tilde{l}\lambda}$ and by subsequently using the fact that the Wronskian of $\tilde{f}_{\tilde{l}}$ and $\tilde{g}_{\tilde{l}}$ is ξ independent and equal to $1/\pi$ (see AJR for details). The desired reaction matrix $\boldsymbol{K}$ or the equivalent quantum defect matrix $\boldsymbol{\mu}$ then becomes

$$K_{\tilde{l}\tilde{l}'}^{(\lambda)}(\epsilon,R) \equiv \tan\pi\mu_{\tilde{l}\tilde{l}'}^{(\lambda)}(\epsilon,R) = \sum_\beta J_{\tilde{l}\beta}(\epsilon)I_{\beta\tilde{l}'}^{-1}(\epsilon). \tag{2.12}$$

The tan function in equation (2.12) is taken for each element individually.

The reaction matrix equation (2.12) can now be used as the input to a generalized multichannel quantum defect treatment. Bound states are found by writing a general superposition of asymptotic channel functions expressed in terms of $\boldsymbol{K}$ which now

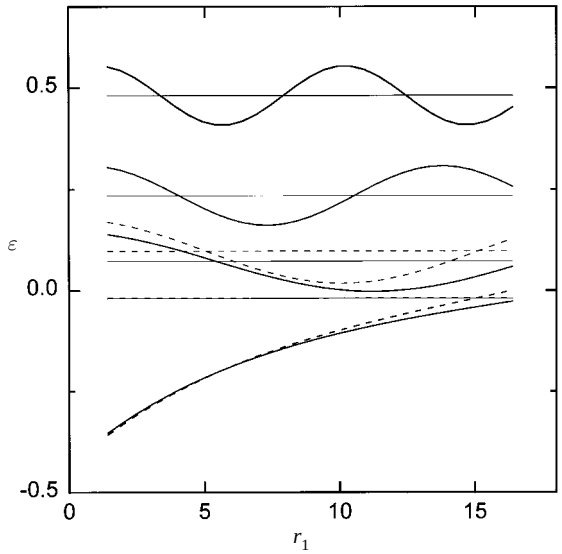

Figure 3. Radial box basis states ($l = 0$) for the R matrix calculation of KrH. The states shown correspond to fixed logarithmic derivatives on both box boundaries. For $r_1 = r_{1a}$ the condition is chosen such as to ensure the continuity of the electron wavefunction ψ_l and of its derivative across the boundary of the Kr atom. For $r_1 = r_{1b}$ the condition is alternatively $-\psi_l'/\psi_l = +1$ (full levels) or -1 (broken levels), as required by the variational R matrix procedure (cf. the text).

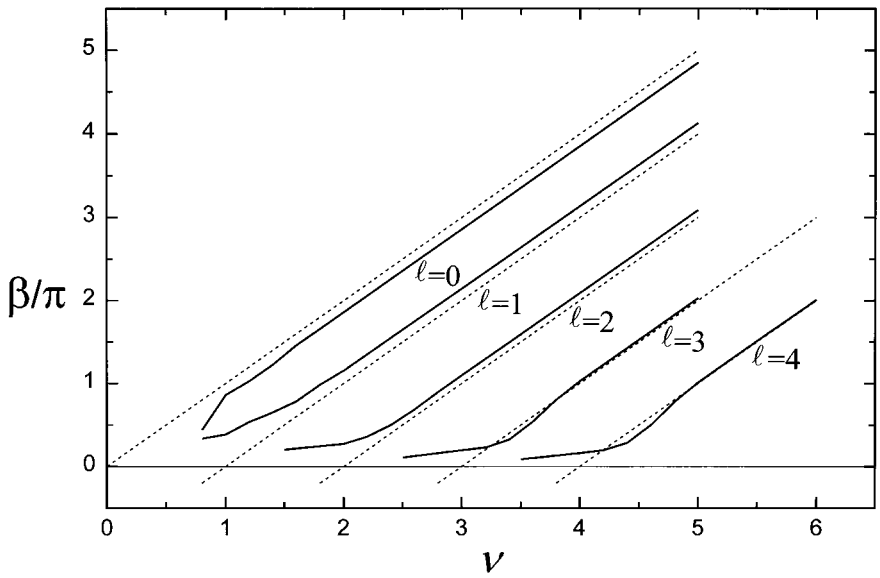

Figure 4. Accumulated phase parameter β, in units of π, plotted as a function of the effective principal quantum number $\nu = (-\epsilon)^{-1/2}$ for $\tilde{l} = 0$–4 and $\lambda = 0$. Full lines: numerical values calculated with the potential equation (2.8) with parameters for KrH from table 2 and $Z_1 = 0$, $Z_2 = +1$. The dotted lines correspond to the phase parameter $\beta/\pi = \nu - l$ for a Coulomb field, used in ordinary quantum defect theory.

embodies all short-range scattering effect in regions II and I. Thus,

$$\Psi(\epsilon) = \sum_{\tilde{l},\tilde{l}'} \tilde{Y}_{\tilde{l}\lambda} \frac{1}{\sqrt{\xi^2 - 1}} [\tilde{f}_{\tilde{l}}(\epsilon, \xi)\delta_{\tilde{l}\tilde{l}'} - \tilde{g}_{\tilde{l}}(\epsilon, \xi)K_{\tilde{l}\tilde{l}'}]Z_{\tilde{l}'}(\epsilon). \tag{2.13}$$

The expansion coefficients $Z_{\tilde{l}}(\epsilon)$ must be chosen such that $\Psi(\epsilon) \to 0$ for $\xi \to \infty$. This leads to the familiar homogeneous linear system of MQDT (see, for example, Seaton 1983), namely,

$$\sum_{\tilde{l}'}[\tan\beta_{\tilde{l}}(\epsilon)\delta_{\tilde{l}\tilde{l}'} + K_{\tilde{l}\tilde{l}'}]Z_{\tilde{l}'}(\epsilon) = 0, \tag{2.14}$$

for each $\tilde{l}$. Non-trivial solutions of equation (2.14) exist when the corresponding determinant is zero. Such zeros occur only for discrete values of the energy, $\epsilon_n = -1/\nu_n^2$, for each value of λ. The corresponding defects $\mu_n = -\nu_n(\mathrm{mod}\,1)$ will be referred to below as 'effective quantum defects'. The coefficients $Z_{\tilde{l}'}(\epsilon_n)$ give the channel mixing for each bound state. $\beta_{\tilde{l}}(\epsilon)$ in equation (2.14) is the accumulated phase parameter for each channel $\tilde{l}$ (whose dependence on λ and R is again not indicated for the sake of clarity). This quantity measures the (generally non-integral) number of half-oscillations of the radial wavefunction at the energy ϵ and is the analogue of the familiar effective principal quantum number ν (times π) in the QDT for pure Coulombic fields. As indicated in AJR, this generalized effective principal quantum number must be evaluated numerically for each required energy in terms of the functions $\tilde{f}$ and $\tilde{g}$.

Figure 4 illustrates the accumulated phase $\beta_{\tilde{l}}$ as a function of $\nu = (-\epsilon)^{-1/2}$ for various $\tilde{l}$ values and $\lambda = 0$ for KrH (full lines). For comparison the familiar analytic Coulombic phase parameter is also shown (dotted lines). If $\boldsymbol{K}$ is neglected in equation (2.14), energy eigenvalues occur whenever β/π is an integer $\geqslant 1$. As illustrated by figure 4, this happens for a pure Coulomb field for integral $\nu = (-\epsilon)^{-1/2}$ (hydrogen atom levels), whereas for KrH the generalized QDT yields near-hydrogenic energies for $\tilde{l} \geqslant 3$, but characteristic $\tilde{l}$-dependent deviations for $\tilde{l} = 0, 1$ and 2 which result from the combined effect of the asymptotic dipole, quadrupole and higher multipole moments, as well as polarization effects. The actual state energies depend, in addition, on the non-diagonal matrix $\boldsymbol{K}$ whose evaluation was the main subject of this section.

3. Details of calculations

(*a*) *Effective electron rare gas atom collision energy*

The potential energy of the molecular electron near the rare gas atom is obtained by setting in equation (2.2) $r_2 \approx R \geqslant r_{2c}$, $\theta_2 \approx 0$ and taking the mean values of $\sin\theta_1$ and $\cos\theta_1$ near the rare gas nucleus to be zero. Thus the classical kinetic energy becomes

$$\epsilon - V_l(\boldsymbol{r}_1, \boldsymbol{r}_2, R) \approx \left[\epsilon + \frac{2Z_2}{R} + \frac{\alpha_2}{R^4}\left(1 - 2Z_1 + 4\frac{\alpha_1 f_1 Z_2}{R^3}\right)\right] - \left[-\frac{2Z_1}{r_1} - \frac{\alpha_1}{r_1^4}f_1^2\right]. \tag{3.1}$$

The second bracket $[\cdots]$ (with $Z_1 = 0$) is just the polarization potential of the rare gas atom, while the r_1-independent first bracket (with α_2 set to zero) represents an effective collision energy

$$\epsilon_1 = \epsilon + \frac{2Z_2}{R}. \tag{3.2}$$

Equation (3.2) relates the molecular electron energy ϵ to the 'local' atomic collision energy ϵ_1. With $Z_2 = +1$ and $\epsilon \geqslant -0.5$ Ry, the effective collision energy turns out to be positive as physically, of course, one expects. Specifically, if we are interested

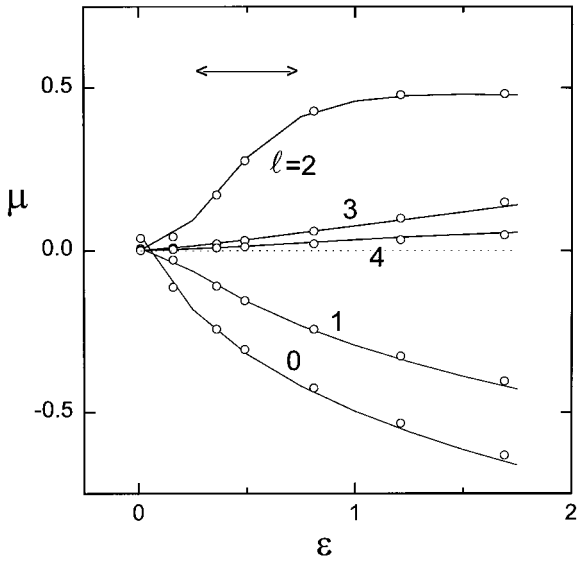

Figure 5. Elastic scattering phase shifts (in units of π) for $Kr \cdot e^-$. The energy (abscissa) is in Rydbergs. Circles: *ab initio* values from McEachran & Stauffer (1984). Full lines: values recalculated with the pseudo-potential equation (3.3) and the parameter values from table 2. The double-headed arrow indicates the range of effective collision energies (equation (3.2)) which is relevant to the bound state spectrum of KrH.

in bound states of RgH between $\nu \approx 1.5$ and ∞ with $\epsilon = -1/\nu^2$, the corresponding electron-rare gas atom collision energy ϵ_1 ranges from *ca.* +0.3 to *ca.* +0.8 Ry.

(*b*) *Logarithmic derivatives* $-b_l(r_{1a})$

The logarithmic derivatives $-b_l(r_{1a})$ of equation (2.1) are the main dynamical parameters of the problem. We determine them from the *ab initio* elastic electron-rare gas atom scattering phase shifts of McEachran & Stauffer (1983, 1984).

In a first step we determine a set of single electron–atom interaction potentials $V_l^{(\mathrm{core})}(r_1)$ which model the screening of the nucleus by the core electrons. The pseudo-potentials are taken to have the following form

$$V_l^{(\mathrm{core})}(r_1) = -\frac{2}{r_1}[(Z_{\mathrm{n1}} - Z_1)\mathrm{e}^{-a_1^{(l)} r_1} + b_1^{(l)} r_1 \mathrm{e}^{-c_1^{(l)} r_1}] + \frac{\alpha_1}{r_1^4}[\mathrm{e}^{(r_1/r_{1\mathrm{c}}^{(l)})^6} - \mathrm{e}^{-(r_1/r_{1\mathrm{c}})^6}]. \quad (3.3)$$

Z_{n1} is the charge of the bare rare gas nucleus while $Z_1 = 0$ is the net charge of the rare gas atom. The first two terms in equation (3.3) represent the screening, while the last term makes the polarization potential cut-off l dependent. The pseudo-character of the potential $V_l^{(\mathrm{core})}$ comes in through the l dependence of the parameters $a_1^{(l)}$, $b_1^{(l)}$, $c_1^{(l)}$ and $r_{1\mathrm{c}}^{(l)}$. $V_l^{(\mathrm{core})}(r_1)$ is defined for all $r_1 \geqslant 0$ and is added to the long-range polarization potential $V^{(P)}(r_1) \approx -(\alpha_1/r_1^4) f_1^2(r_1)$ from equation (3.1). $V_l^{(\mathrm{core})}$ becomes exponentially small outside the rare gas atom ($r_1 \geqslant (a_1^{(l)})^{-1}$, $(c_1^{(l)})^{-1}$, $r_{1\mathrm{c}}^{(l)}$), but we do add its tail to the potential in zone II as indicated in equation (2.2). We have fitted the values of the parameters $a_1^{(l)}$, $b_1^{(l)}$, $c_1^{(l)}$ and $r_{1\mathrm{c}}^{(l)}$ in a least-squares treatment in such a way that for each l value the combined effective potential $V^{(P)}(r_1) + V_l^{(\mathrm{core})}(r_1) + l(l+1)/r_1^2$ represents the energy-dependent *ab initio* elastic scattering phase shifts as accurately as possible. The resulting pseudo-potential parameters for Ar and Kr are listed in table 2. Figure 5 illustrates the agreement

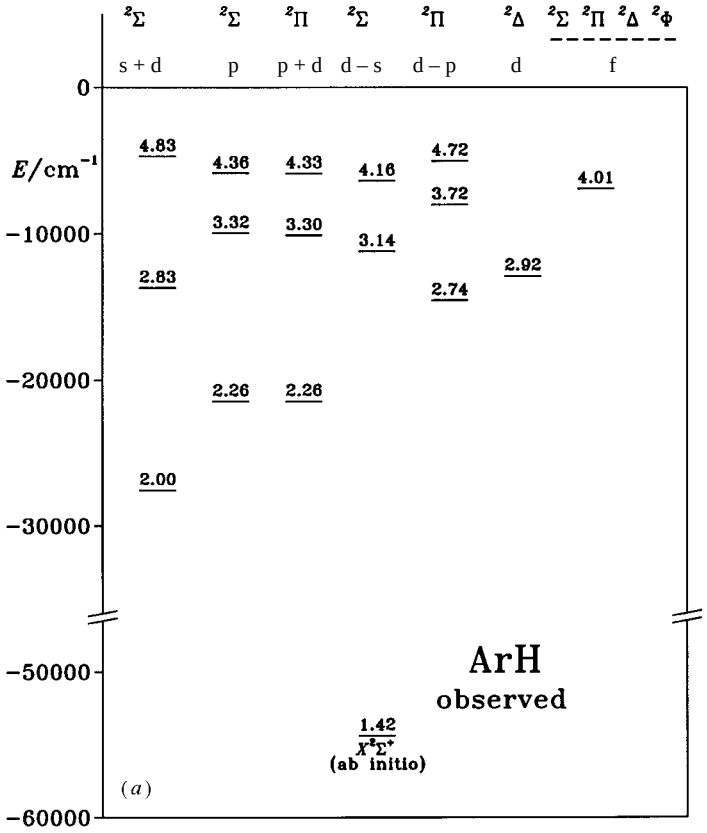

Figure 6. Energy level diagram for ArH: (*a*) observed.

between the *ab initio* phase shifts (circles) and those recalculated by numerical integration of the radial Schrödinger equation with the parameters from table 2 (lines) for Kr. The energy range relevant to the Rydberg spectrum of the hydride (cf. equation (3.2)) is indicated in figure 5 by a double-headed arrow. Notice the strong energy dependence of the $l = 0$, 1 and 2 phase shifts in this region.

Using the pseudo-potentials thus defined, we now obtain each $b_l(r_{1a})$ (equation (2.1)) by straightforward outward numerical integration of the radial Schrödinger equation in this potential from $r_1 = 0$ to $r_1 = r_{1a}$. We have taken $r_{1a} = 1.4$ both for Ar and Kr and we have checked that the results of the calculation do not critically depend upon this choice.

(*c*) *Rare gas polarizabilities and core dipole moment*

Within the framework of our model the rare gas atom dipole polarizability is related by equation (2.10*b*) to the dipole moment of the corresponding rare gas hydride ion core. The polarizabilities of the rare gases are known (cf. table 1) and so are the ion core dipole moments which have been calculated *ab initio* by Klein & Rosmus (1984). By inverting equation (2.10*b*) and using their calculated dipole moments, we can thus determine a set of 'effective' rare gas atom polarizabilities which are appropriate for the atoms within the molecular environment. The *ab initio* dipole moment values Q_1 and the hence determined effective polarizabilities $\alpha_d^{(\mathrm{eff})}$ are listed in the second-to-last and in the last column of table 1, respectively. It can be

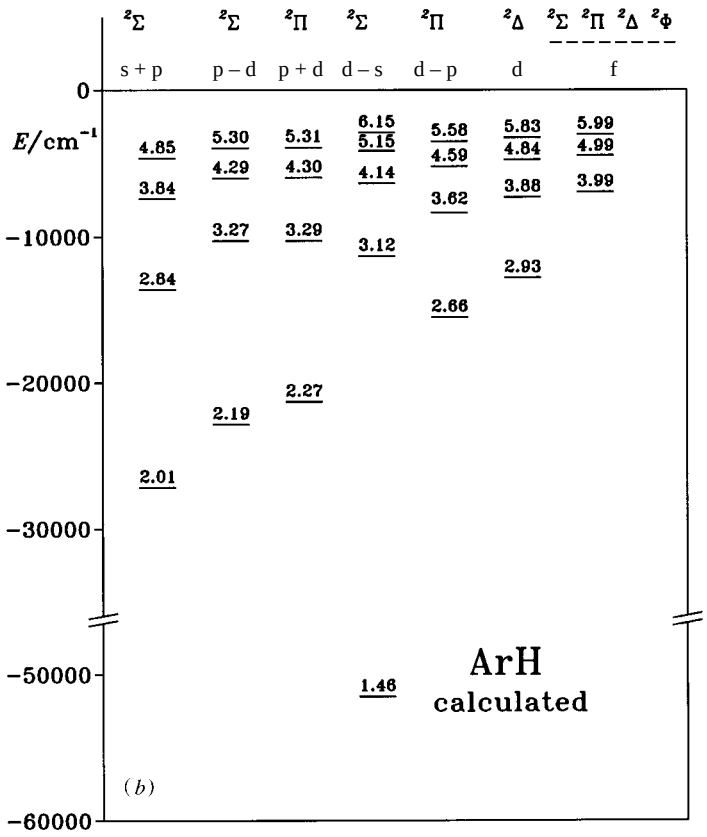

Figure 6. Energy level diagram for ArH: (*b*) calculated.

seen that while the polarizability increases by a factor of 20 between He and Xe, the effective values obtained with equation (2.10 *b*) are consistently close to the free atom values, thus lending support to the assumption that the molecular ions RgH^+ can be viewed as protonated rare gas atoms. Table 1 shows further that the 'effective' values are systematically about 17% lower than the free atom values, indicating that an atom-independent saturation effect occurs in the molecular rare gas hydride cores similar to that found previously in the alkaline earth halides (cf. the discussion in AJR).

In our calculations we used the reduced effective values $\alpha_d^{(\mathrm{eff})}$ both in the pseudopotential equation (3.3) which defines the boundary condition at $r_1 = r_{1\mathrm{a}}$ and in the molecular electron potential equation (2.2). Finally we took $r_{1\mathrm{c}}$ equal to $r_{1\mathrm{c}}^{(l=0)}$ (cf. equations (2.3) and (3.3)). The internuclear distance was taken as given in table 1.

(*d*) *R-matrix radii* $r_{1\mathrm{b}}$, ξ_0 *and basis sets*

The outer R matrix radii $r_{1\mathrm{b}}$, ξ_0 and the basis sets equation (2.4) have been chosen based on considerations and tests similar as detailed in AJR. The final calculations were carried out with $r_{1\mathrm{b}} = 12.08a_0$ and $\xi_0 = 8.0$. The angular basis included values $l = \lambda - 4$ with 19 radial functions with $b_l(r_{1\mathrm{b}}) = +1.0$ and 2 functions with $b_l(r_{1\mathrm{b}}) = -1.0$ for each l value.

Table 3. (*a*) $^2\Sigma^+$ *Rydberg series of ArH*

(The ionization potential of the lowest stable state of ArH (ArD) is 27 530 cm^{-1} (27 570 cm^{-1})[a,b]. Each series is designated by ν (mod 1) of the highest observed state. The spectral composition of each series is given for $\nu \approx 5$.)

0.83 $^2\Sigma^+$ $0.65\tilde{s}+0.57\tilde{p}+0.49\tilde{d}$			0.33 $^2\Sigma^+$ $0.81\tilde{p}-0.42\tilde{d}-0.37\tilde{s}$			0.16 $^2\Sigma^+$ $0.74\tilde{d}-0.66\tilde{s}+0.11\tilde{f}$			0.97 $^2\Sigma^+$ $0.97\tilde{f}-0.21\tilde{d}$		
ν_{obs}	ν_{calc}	o − c	ν_{obs}	ν_{calc}	o − c	ν_{obs}	ν_{calc}	o − c	ν_{obs}	ν_{calc}	o − c
2.00[a]	2.01	−0.01	2.26[a]	2.19	+0.07		1.54		3.97[b]	3.98	−0.01
2.83[a]	2.84	−0.01	3.31[b]	3.27	+0.04	3.14[a]	3.12	+0.02		4.97	
	3.84		4.33[b]	4.29	+0.04	4.16[a]	4.14	+0.02		5.97	
4.83[b]	4.85	−0.02		5.30			5.15			6.97	
	5.85			6.30			6.15				
	6.85						7.15				

[a]Data for ArH (Dabrowski *et al.* 1997*a*, *b*).
[b]Data for ArD (Dabrowski *et al.* 1997*a*, *b*).

Table 3. (*b*) $^2\Pi$ *Rydberg series of ArH*

(See table 3*a* for notation.)

0.31 $^2\Pi$ $0.93\tilde{p}+0.36\tilde{d}$			0.69 $^2\Pi$ $0.91\tilde{d}-0.36\tilde{p}+0.18\tilde{f}$			0.98 $^2\Pi$ $0.98\tilde{f}-0.18\tilde{d}$		
ν_{obs}	ν_{calc}	o − c	ν_{obs}	ν_{calc}	o − c	ν_{obs}	ν_{calc}	o − c
2.26[a]	2.27	−0.01	2.74[a]	2.66	+0.08	3.98[b]	3.98	+0.00
3.29[b]	3.29	+0.00	3.71[b]	3.62	+0.09		4.97	
4.31[b]	4.30	+0.01	4.69[b]	4.59	+0.10		5.97	
	5.31			5.58			6.97	
	6.31			6.58				

Table 3. (*c*) $^2\Delta$ *Rydberg series of ArH*

(See table 3*a* for notation.)

0.92 $^2\Delta$ $0.98\tilde{d}+0.22\tilde{f}$			0.99 $^2\Delta$ $0.98\tilde{f}-0.22\tilde{d}$		
ν_{obs}	ν_{calc}	o − c	ν_{obs}	ν_{calc}	o − c
2.92[a]	2.93	−0.01	3.99[b]	3.99	+0.00
	3.88			4.99	
	4.84			5.99	
	5.83			6.99	
	6.83				

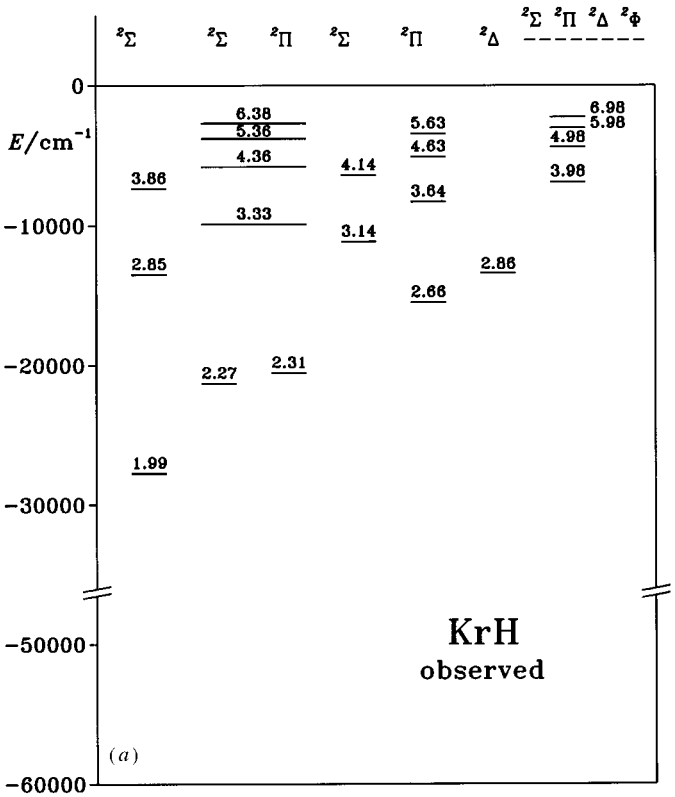

Figure 7. Energy level diagram for KrH: (*a*) observed.

Table 3. (*d*) $^2\Phi$ *Rydberg series of ArH*
(See table 3*a* for notation.)

$0.02\ ^2\Phi$ $1.00\tilde{f}$		
ν_{obs}	ν_{calc}	o − c
4.02[b]	4.01	+0.01
	5.01	
	6.01	

4. Results

(*a*) *Rydberg series*

Tables 3 and 4 summarize the effective principal quantum numbers ν_n obtained for the various values of λ for KrH and ArH and compare them with the corresponding experimental values. The same data are represented graphically in the energy level diagrams of Figures 6 (ArH) and 7 (KrH) and in the $\nu(\mathrm{mod}\,1)$ versus ν plots of figure 8 (ArH) and figure 9 (KrH). The quantity $\nu(\mathrm{mod}\,1)$ (ordinate) is the effective principal quantum number stripped of its integral part in front of the decimal point

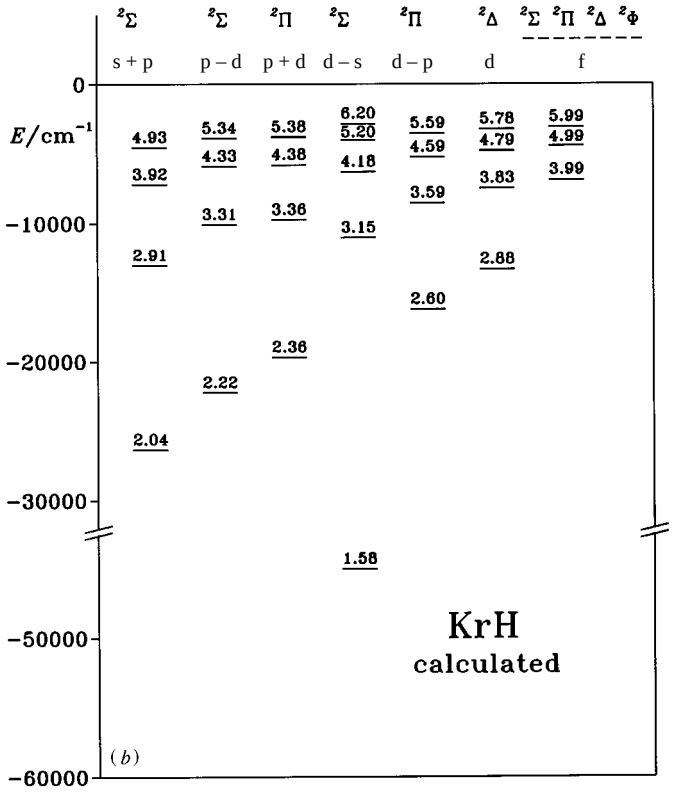

Figure 7. Energy level diagram for KrH: (*b*) calculated.

and corresponds to the negative of the effective quantum defect. Per unit interval of ν, this quantity provides an enlarged view of the relative positions of the states.

Tables 3 and 4 and the effective quantum defect plots of figures 8 and 9 show that the agreement between experiment and calculations is on the whole quite good. The calculations predict correctly where the lowest state of each series occurs, i.e. which is its 'terminus' state. The characteristic energy dependences at low ν, showing up in figures 8 and 9 as curvatures of some of the quantum defect curves, are also correctly reproduced. The mean deviation $|\nu_{\mathrm{obs}} - \nu_{\mathrm{calc}}|$ is 0.043 for ArH (19 electronic states) and 0.036 for KrH (24 electronic states). The agreement is thus about a factor 1.5 worse than we found previously for CaF and BaF. The worst discrepancies occur for the 0.69 $^2\Pi$ and the 0.33 $^2\Sigma^+$ series of ArH which are calculated too low by $\Delta\nu \approx 0.09$ and 0.05, respectively.

The main components $\tilde{l}'$ occurring in the expansion equation (2.13) for $\nu \approx 5$ are listed for each series in tables 3 and 4. As expected, most of the series are strongly $\tilde{l}$ mixed. Note that this mixing occurs in addition to the mixing due to the asymptotic multipole field which causes each elliptic component $\tilde{l}$ to be itself a mixture of spherical partial waves l. Thus it is clear that at least for low l it is not possible to assign even approximate l values to the individual series. We note nevertheless that the largest coefficients listed in tables 3 and 4 for the various series correspond in all cases to $\tilde{l}$ values identical with the l assignments made by Dabrowski *et al.* (1996) for ArH and by Dabrowski & Sadovskii (1994) for KrH. Our

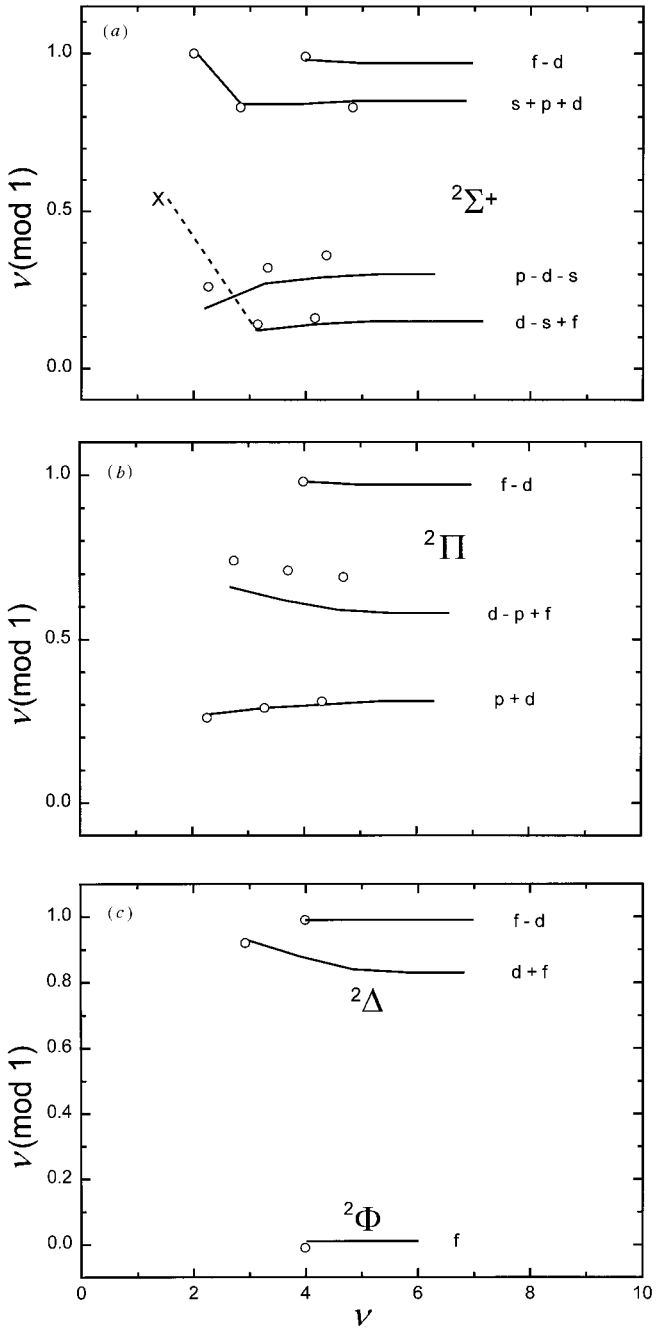

Figure 8. Rydberg series of ArH. $\nu(\mathrm{mod}\,1)$ of bound states is plotted versus ν, where ν is the effective principal quantum number and $\nu(\mathrm{mod}\,1) = -\mu$ with μ the effective quantum defect. The abscissa thus represents the electron binding energy on the gross nonlinear scale $\nu = (-\epsilon)^{-1/2}$. For each unit interval the same information is represented on the ordinate on an enlarged scale. The spectral composition of each series for high ν in terms of elliptic components $\tilde{l}$ is indicated on the right. Circles: observed values. Full lines: calculated values. The value of the unstable ground state, marked X, corresponds to the vertical ionization energy calculated for $R = R_e^+$. (*a*) $^2\Sigma$ states. (*b*) $^2\Pi$ states. (*c*) $^2\Delta$ states and $^2\Phi$ states.

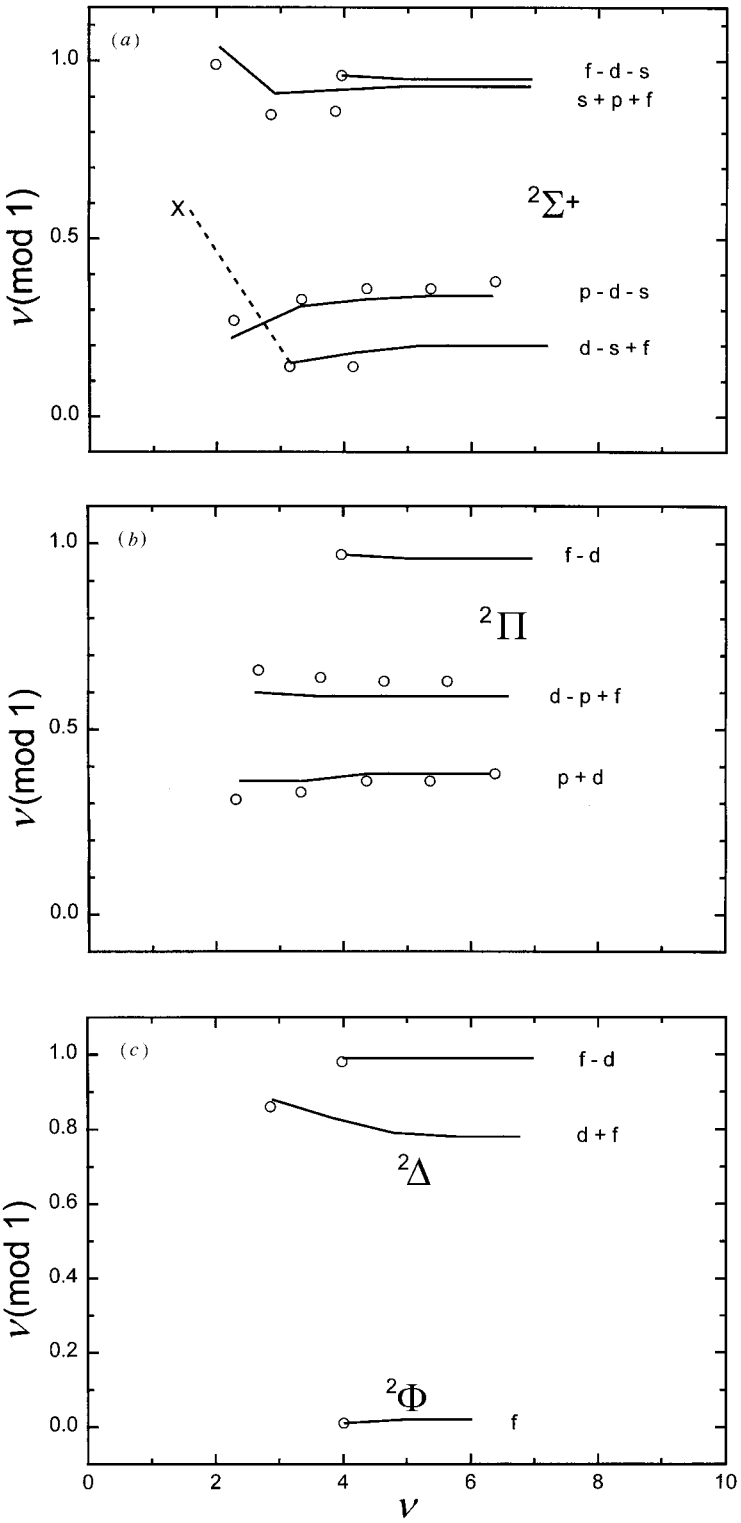

Figure 9. Rydberg series of KrH (cf. caption for figure 8).

Table 4. (*a*) $^2\Sigma^+$ *Rydberg series of KrH*

(The ionization potential of the lowest stable state of KrD is 27 727 cm^{-1}[a]. Each series is designated by ν (mod 1) of the highest observed state. The spectral composition of each series is given for $\nu \approx 5$.)

0.86 $^2\Sigma^+$ $0.61\tilde{s}+0.50\tilde{p}+0.46\tilde{f}$			0.38 $^2\Sigma^+$ $0.86\tilde{p}-0.35\tilde{d}-0.33\tilde{s}$			0.14 $^2\Sigma^+$ $0.75\tilde{d}-0.65\tilde{s}+0.11\tilde{f}$			0.96 $^2\Sigma^+$ $0.86\tilde{f}-0.38\tilde{d}-0.31\tilde{s}$		
ν_{obs}	ν_{calc}	o − c	ν_{obs}	ν_{calc}	o − c	ν_{obs}	ν_{calc}	o − c	ν_{obs}	ν_{calc}	o − c
1.99[a]	2.04	−0.05	2.27[a]	2.22	+0.05		1.58		3.96[b]	3.96	+0.00
2.85[a]	2.91	−0.06	3.33[a]	3.31	+0.02	3.14[a]	3.15	−0.01		4.95	
3.86[a]	3.92	−0.06	4.36[a]	4.33	+0.03	4.14[a]	4.18	−0.04		5.95	
	4.93		5.36[a]	5.34	+0.02		5.20			6.95	
	5.93		6.38[a]	6.34	+0.04		6.20				
	6.93						7.20				

[a]Data for KrD (Dabrowski & Sadovskii 1994).
[b]Data for KrD (Dabrowski *et al.* 1997*a*, *b*).

Table 4. (*b*) $^2\Pi$ *Rydberg series of KrH*

(See table 4*a* for notation.)

0.38 $^2\Pi$ $0.95\tilde{p}+0.31\tilde{d}$			0.63 $^2\Pi$ $0.93\tilde{d}-0.30\tilde{p}+0.22\tilde{f}$			0.97 $^2\Pi$ $0.98\tilde{f}-0.21\tilde{d}$		
ν_{obs}	ν_{calc}	o − c	ν_{obs}	ν_{calc}	o − c	ν_{obs}	ν_{calc}	o − c
2.31[a]	2.36	−0.05	2.66[a]	2.60	+0.06	3.97[b]	3.97	+0.00
3.33[a]	3.36	−0.03	3.64[a]	3.59	+0.05		4.96	
4.36[a]	4.38	−0.02	4.63[a]	4.59	+0.04		5.96	
5.36[a]	5.38	−0.02	5.63[a]	5.59	+0.04		6.96	
6.38[a]	6.38	+0.00		6.59				

Table 4. (*c*) $^2\Delta$ *Rydberg series of KrH*

(See table 4*a* for notation.)

0.86 $^2\Delta$ $0.97\tilde{d}+0.25\tilde{f}$			0.98 $^2\Delta$ $0.97\tilde{f}-0.25\tilde{d}$		
ν_{obs}	ν_{calc}	o − c	ν_{obs}	ν_{calc}	o − c
2.86[a]	2.88	−0.02	3.98[b]	3.99	−0.01
	3.83			4.99	
	4.79			5.99	
	5.78			6.99	
	6.78				

Table 4. (*d*) $^2\Phi$ *Rydberg series of KrH*
(See table 4*a* for notation.)

	$0.01\ ^2\Phi$ $1.00\tilde{f}$		
	$\nu_{\rm obs}$	$\nu_{\rm calc}$	o − c
	4.01[b]	4.01	−0.00
		5.02	
		6.02	

Table 5. *The lowest electronic states of ArH* (cm^{-1})

		present		*ab initio*	
	obs[a], T_0	calc[b]	o − c	calc[c]	o − c
$X\ ^2\Sigma^+$		−23951[d]		−26859	
$2.00\ ^2\Sigma^+$	0	368	−368	0	0
$2.26\ ^2\Sigma^+$	6092	4649	+1443	5323	+769
$2.26\ ^2\Pi$	6074	6234	−160	4839	+1235
$2.74\ ^2\Pi$	12905	12021	+884	12583	+322
$2.83\ ^2\Sigma^+$	13783	13924	−141	12583	+1200
$2.92\ ^2\Delta$	14634	14747	−113	14115	+519
mean deviation			714		809

[a]Data for ArH (Dabrowski *et al.* 1997*a*, *b*).
[b]$R = 2.43\ a_0$. Values obtained from the theoretical ν_n values and the experimental IP from table 3.
[c]$R = 2.50\ a_0$ (Petsalakis & Theodorakopoulos 1994).
[d]$R = 2.50\ a_0$, $\nu = 1.46$.

calculations thus confirm the l assignments of these authors and, in particular, the revision proposed in 1994 for KrH.

The energy level diagrams of figures 6 and 7 illustrate the occurrence of 'pseudo-l complexes' in the rare gas hydrides. The systematic near degeneracies of the $n.33\ ^2\Sigma^+$ and $n.31\ ^2\Pi$ 'p'-type pairs of states are correctly reproduced, although the calculations are not accurate enough to account quantitatively for the small $^2\Sigma$–$^2\Pi$ splittings. By contrast, the larger $^2\Sigma$–$^2\Pi$–$^2\Delta$ splittings of the 'd'-type triplets are calculated correctly. The f series are discussed separately in § 4 *c*.

(*b*) *Low electronic states*

Tables 5 and 6 compare the observed and calculated energies (in wavenumber units) of the lowest six stable states of ArH and KrH. In the case of ArH (table 5), the latest MRD-CI *ab initio* calculations of Petsalakis & Theodorakopoulos (1994) are also included. The mean deviation observed–calculated is of the order of 0.1 eV both for ArH and KrH, for our calculations as well as the *ab initio* work.

Table 5 also compares our calculated value of the energy of the repulsive ArH

Table 6. *The lowest electronic states of KrH* (cm^{-1})

		present	
	obs[a], T_0	calc[b]	o − c
$X\ ^2\Sigma^+$		−16231	
$1.99\ ^2\Sigma^+$	0	1358	−1358
$2.27\ ^2\Sigma^+$	6480	5461	+1019
$2.31\ ^2\Pi$	7216	8024	−808
$2.66\ ^2\Pi$	12280	11494	+786
$2.85\ ^2\Sigma^+$	14205	14768	−563
$2.86\ ^2\Delta$	14250	14497	−247
mean deviation			869

[a]Data for KrD (Dabrowski & Sadovskii 1994).
[b]$R = 2.68\ a_0$. Values obtained from the theoretical ν_n values and the experimental IP from table 4.

$X\ ^2\Sigma^+$ ground state at $R = 2.5$ a.u. with the *ab initio* value of Petsalakis & Theodorakopoulos (1994) which is seen to be about 2900 cm^{-1} lower than ours. This shows that even the ground state is semi-quantitatively reproduced by our model. The difference between the two calculations in terms of ν amounts to 0.04. No obvious association of $X\ ^2\Sigma^+$ with any of the $^2\Sigma^+$ series of ArH and KrH is apparent in the quantum defect plots of figures 8*a* and 9*a*. According to the calculation the ground states of the two molecules correspond to an antisymmetric linear combination of $\tilde{d}$ and $\tilde{s}$ waves and for this reason we have formally associated X with the $0.16\ ^2\Sigma^+$ ($0.14\ ^2\Sigma^+$) series of ArH (KrH) in the tables and figures.

(*c*) *λ structure in the f complexes*

A feature of particular interest is the λ structure of the quantum defects associated with the nearly non-penetrating 4f electrons in ArH and KrH.

It has been known for a long time that in homopolar diatomic molecules the splittings of the λ components of the states with $l \geqslant 3$ is for the most part due to the core quadrupole and depends on the sign of the latter. More recently, Zon (1992) and Watson (1994) showed that the dipole field in dipolar systems also contributes and that this contribution arises in second-order perturbation theory and therefore is proportional to the square of the dipole moment. For total core charge $Z = Z_1 + Z_2 = 1$ the expression for the quantum defect μ is (Watson 1994)

$$\mu_{l,\lambda} = -\frac{2[l(l+1) - 3\lambda^2]}{(2l+3)(2l+1)(2l-1)l(l+1)}(Q_1^2 - Q_2), \tag{4.1}$$

where Q_2 is the quadrupole moment and the combination $(Q_1^2 - Q_2)$ is independent of the choice of origin. According to equation (4.1) the dipole field always tends to push the component $l, \lambda = 0$ up highest (negative quantum defect) and the $l, \lambda = l$ component down lowest (positive quantum defect). As discussed in detail in AJR, the alkaline earth halides are examples where the dipole field dominates by far. ArH and KrH are also rather strongly dipolar systems, but the ordering of the observed and

calculated λ components given in tables 3 and 4 tells us that in the rare gas hydrides the (positive) quadrupole moment is more important than the dipole moment.

The quantitative agreement between observations and calculations for the λ structure of the 4f complexes is quite reasonable both for ArH and KrH as an inspection of tables 3 and 4 shows. The observed (calculated) overall splitting $\nu(4f\phi)$–$\nu(4f\sigma)$ is +0.06 (+0.05), respectively, for KrH, and the observed (calculated) mean position of all the substates is 3.98 (3.99), respectively. (The degenerate states with $\lambda > 0$ have been counted twice here.) The corresponding observed (calculated) values for the overall splitting in ArH are +0.05 (+0.03), respectively, and 3.99 (3.99) for the mean ν value. The agreement thus obtained for these largely non-penetrating $\tilde{l} = 3$ states indicates that our description of the asymptotic core field must be about correct. At the same time the spectral composition of these states given in tables 3 and 4 shows that significant l mixing is also present in spite of the relatively high $\tilde{l}$ value. Indeed, unlike in CaF and BaF, equation (4.1) with Q_1 and Q_2 evaluated according to the prescription of equation (2.10), is not a good approximation for the rare gas hydrides and accounts for only about half of the observed overall splittings of the 4f complexes. Note that the groups of states assigned to a d electron do not exhibit any such simple ordering relationship: the energy level diagrams of figures 6 and 7 show the δ above the π component for $\nu \approx 3$ in line with what we expect for a positive quadrupole field, whereas the σ component (which should be lowest) is pushed up highest due to interaction with the low-lying X precursor.

5. Spherical quantum defect matrices

The quantum defect theory of rovibronic Rydberg fine structure is based on transformations from the body-fixed to the laboratory frame which allow the non-adiabatic couplings between electronic and nuclear motions to be taken into account in an elegant fashion. In practice the rovibronic quantum defect matrices are evaluated from the purely electronic body-fixed matrices through a folding process with the appropriate frame transfomation matrices (see papers on this subject reprinted in Jungen (1996)). In particular, the rotational transformation matrices are expressed in terms of vector coupling coefficients. The elliptical electronic quantum defect matrices $\mu_{\tilde{l},\tilde{l}'}$ used in the present work for the calculation of the electronic structure can thus not be transferred directly to the frame transformation scheme.

We return at this point to the R-matrix solutions Ψ_β of equation (2.6) and their elliptical asymptotic form equation (2.11). This latter equation is valid for any $\xi \geqslant \xi_0$ with the coefficients $I_{\tilde{l}\beta}$ and $J_{\tilde{l}\beta}$ determined for $\xi = \xi_0$. We thus use equation (2.11) to evaluate the R-matrix eigensolutions on a sphere $r_3 = r_{3c} \geqslant r_{1b}$, centred on the molecular centre of mass, which we chose large enough so that (with $\xi \gg \eta$ and $\xi \approx 2r_3/R$) we have $V \approx 2(Z_1 + Z_2)/r_3$, i.e. only the Coulomb term remains. Then the matching procedure, equations (2.11)–(2.12), may be repeated with the difference that all the tildes are omitted. Specifically, the asymptotic channel functions are now

$$Y_{l\lambda}(\theta, \phi)\frac{1}{r_3}[f_l(\epsilon, r_3)I_{l\beta}(\epsilon) - g_l(\epsilon, r_3)J_{l\beta}(\epsilon)], \tag{5.1}$$

where the Y are ordinary spherical harmonics and the f_l and g_l are Coulomb radial functions as defined by Seaton (1983) (his functions s and c). The analogue of equation (2.12) now yields *spherical* quantum defect matrices $\mu_{ll'}^{(\lambda)}(\epsilon, R)$ which are appropriate for use in the framework of the customary quantum defect–frame transformation theory.

Table 7. *Spherical quantum defect matrices* $\mu_{l,l'}^{(\lambda)}$ *for ArD*[a]

(The matrix elements involving $l = 4$ (g) channels are all smaller than *ca.* 0.006 and are not given.)

	s	p	d	f
$\lambda = 0$	+0.09	−0.07	+0.11	−0.02
		−0.27	−0.11	+0.04
			−0.13	+0.03
				+0.03
$\lambda = 1$		+0.24	+0.41	−0.15
			+0.42	−0.19
				+0.06
$\lambda = 2$			+0.17	−0.04
				+0.01
$\lambda = 3$				−0.02

[a] $R = 2.43\ a_0$, $\epsilon = -0.04$.

Tables 7 and 8 list the elements of these spherical quantum defect matrices for ArD and KrD which we obtained in this way for an energy corresponding to $\epsilon = -0.040$ ($\nu = 5$). We found that r_{3c} had to be taken of the order of *ca.* 50 a.u. in order to obtain convergence. This radius gives us an idea of the 'real' size of the molecular ion core, corresponding to the volume within which significant departures from the field of an electric point charge occur. Note that a direct evaluation of the spherical quantum defect matrix by an R-matrix calculation with $r_b = r_{3c}$ would require a vastly increased amount of computer time. We carried out similar calculations for $\epsilon = -0.009$ and $\epsilon = +0.040$ and we found that the spherical μ matrices vary little with energy. The matrices of tables 7 and 8 yield, when entered into the spherical version of the secular equation (2.14) (Coulombic phase parameters $\beta(\epsilon)$ such as represented by dotted lines in figure 4), the same eigenvalues ν_n near $\nu \approx 5$ as are listed in tables 3 and 4. The matrices of table 7 are used in the work of Dabrowski *et al.* (1997*a*, *b*) for the interpretation of the rotational fine structure of the 4f group of states of KrD.

6. Discussion and conclusion

This work, together with that of AJR, has shown that our generalized ligand-field approach to treat Rydberg molecules with composite double closed shell cores, applies nearly as well to the rare gas monohydrides as to the alkaline earth halides. All these molecules are rather strongly dipolar and most of the states calculated have been found to be strongly l mixed. One reason for the success of the calculations is no doubt the fact that asymptotically we are using elliptical angular and radial basis functions which have the effects of the long-range dipole field fully built into them. Thus we have been able to carry out the R-matrix calculations rather efficiently in a restricted zone whose radius is only about 10 a.u..

The fact that the agreement between theory and experiment is not quite as good as we found previously for CaF and BaF does not necessarily mean that our scattering model is less appropriate for the rare gas hydrides than it was for the alkaline earth

Table 8. *Spherical quantum defect matrices* $\mu_{l,l'}^{(\lambda)}$ *for KrD*[a]

(The matrix elements involving $l = 4$ (g) channels are all smaller than *ca.* 0.006 and are not given.)

	s	p	d	f
$\lambda = 0$	+0.01	−0.03	+0.11	−0.02
		−0.32	−0.13	+0.05
			−0.19	+0.03
				+0.04
$\lambda = 1$		−0.41	+0.33	+0.02
			+0.30	−0.09
				+0.05
$\lambda = 2$			+0.23	−0.05
				+0.02
$\lambda = 3$				−0.02

[a] $R = 2.68\ a_0$, $\epsilon = -0.04$.

halides. First of all, the lack of experimental data has not permitted us to convert the experimental T_0 values into vertical ionization energies as this was done by AJR, by taking account of the slight differences between the vibrational frequencies and equilibrium internuclear distances in the lower Rydberg states and the ion. Further, the observed series do not extend to ν values as high as in the alkaline earth halides so that the current values of the ionization potentials may not be as accurate as in the alkaline earth halides. This may affect the higher observed ν values somewhat. More importantly, the present calculations are based on purely theoretical electron-rare gas atom scattering phase shifts and rare gas hydride ion dipole moments, and their success depends crucially on the accuracy of these *ab initio* input data. It is fair to say that by and large our calculations confirm the high quality of the *ab initio* work of McEachran & Stauffer (1983, 1984) and of Klein & Rosmus (1984). We have found, however, that a slight adjustment of the effective rare gas atom polarizability α_1 improves the agreement between experiment and theory for ArH considerably. Substitution of $\alpha_1 = 8.00$ instead of $9.14 a_0^3$ into equations (2.2) and (2.8) moves the calculated 0.33 $^2\Sigma^+$ and 0.69 $^2\Pi$ $\nu(\mathrm{mod}\,1)$ values in figures 8*a* and 8*b* up near the experimental points while affecting all the other series only a little. We do not report these results in detail since our aim here was to test the predictive power of the theory rather than obtaining perfect agreement with experiment at all cost.

Our goal for the future is to use the approach for the calculation of finer details of the electronic structure of the rare gas hydrides as well as of the alkaline earth halides, such as permanent and transition dipole moments, and spin-orbit coupling effects. We also plan to apply the method to polyatomic molecules with composite closed-shell cores such as small van der Waals complexes.

We thank Dr I. Dabrowski and Dr J. K. G. Watson (NRC, Ottawa) for letting us use their results on ArD and KrD before publication.

References

Arif, M., Jungen, Ch. & Roche, A. L. 1997 *J. Chem. Phys.* **106**, 4102–4118.

Cuthbertson, C. & Cuthbertson, A. 1932 *Proc. R. Soc. Lond.* A **135**, 40–47.

Dabrowski, I. & Sadovskii, D. A. 1994 *Molec. Phys.* **81**, 291–326.

Dabrowski, I., Tokaryk, D. W., Vervloet, M. & Watson, J. K. G. 1996 *J. Chem. Phys.* **104**, 8245–8257.

Dabrowski, I., Tokaryk, D. W. & Watson, J. K. G. 1997*a J. Chem. Phys.* (In the press.)

Dabrowski, I., Tokaryk, D. W., Lipson, R. H. & Watson, J. K. G. 1997*b J. Chem. Phys.* (In the press.)

Fano, U. & Lee, C. M. 1973 *Phys. Rev. Lett.* **31**, 1573–1576.

Greene, C. H. 1983 *Phys. Rev.* A **28**, 2209–2216.

Herzberg, G. 1987 *Ann. Phys. Chem.* **38**, 27–56.

Jungen, Ch. 1996 *Molecular applications of quantum defect theory.* Bristol: Institute of Physics Publishing.

Klein, R. & Rosmus, P. 1984 *Z. Naturf.* a **39**, 349–353.

McEachran, R. P. & Stauffer, A. D. 1983 *J. Phys. B: At. Mol. Opt. Phys.* **16**, 4023–4038.

McEachran, R. P. & Stauffer, A. D. 1984 *J. Phys. B: At. Mol. Opt. Phys.* **17**, 2507–2518.

Moore, C. E. 1971 *Atomic energy levels*, vol. I–III. Washington, DC: National Bureau of Standards.

Petsalakis, L. D. & Theodorakopoulos, G. 1994 *J. Phys. B: At. Mol. Opt. Phys.* **27**, 4483–4489.

Rice, S. F., Martin, H. & Field, R. W. 1985 *J. Chem. Phys.* **82**, 5023–5034.

Rosmus, P. 1979 *Theoret. Chim. Acta (Berl.)* **51**, 359–362.

Rosmus, P. & Reinsch, E.-A. 1980 *Z. Naturf.* a **35**, 1066–1070.

Seaton, M. J. 1983 *Rep. Prog. Phys.* **46**, 167–257.

Watson, J. K. G. 1994 *Molec. Phys.* **81**, 277–289.

Zon, B. A. 1992 *Soviet Phys. JETP* **75**, 19–24.

Discussion

M. Child (*Physical and Theoretical Chemistry Laboratory, University of Oxford, UK*). Is there any explanation for the fact that the σ states of BaF seem to be so much more vibrationally perturbed than those for higher λ?

Ch. Jungen. σ orbitals are directed along the molecular axis and therefore are sensitive to displacements of the nuclei. Vibronic interactions are the consequence. In the terms of quantum defect theory one would say that the σ quantum defects have the largest R-dependence.

R. W. Field (*Department of Chemistry, MIT, USA*). Dr Jungen suggested that one of the CaF $v^+ = 0$ $^2\Sigma^+$ states in the $14 < n^* < 15$ region is possibly locally perturbed by a $v^+ = 1$ state and that this is the reason for the larger discrepancies than he found in your fit to the +Kronig symmetry than −Kronig symmetry states. Since all $^2\Sigma^+$ states belong uniquely to +Kronig symmetry (and all $^2\Lambda$ other states exist as a pair of + and −Kronig symmetry substates), deviations unique to +Kronig symmetry are almost certainly due to a special case of interchannel perturbation that affects only Σ^+ states.

He is right! There are intrachannel perturbations of the type $\Delta v^+ = -1$, $\Delta n^* =$ +integer that are due to the internuclear distance dependence of the quantum defect (Herzberg & Jungen 1972). The perturbation matrix element has the form

$$\langle n^*, v^+|\boldsymbol{H}'|-n, v^+ + 1\rangle = [2\,\mathrm{Re}(4.106)(\mu\omega_e^+)^{1/2}]\left(\frac{\mathrm{d}\mu}{\mathrm{d}R}\right)_{R_e^+}[v^+ + 1]^{1/2}[n^*(n^* - n)]^{-3/2},$$

where the first [ ] contains all constants that are needed to give the matrix element

Table 9.

n^*	15.92	14.56	13.12	11.53	9.71	7.37
n	6	5	4	3	2	1

in cm^{-1} and the quantum defect derivative in $\mathrm{Å}^{-1}$ (for CaF^2, the reduced mass, μ, in amu is 12.89 and $\omega_e^+ = 685\,\mathrm{cm}^{-1}$, thus the first factor in [ ] is $9590\,\mathrm{cm}^{-1}\,\mathrm{Å}^{-1}$), $(\mathrm{d}\mu/\mathrm{d}R)_{R_e^+}$ is the quantum defect derivative evaluated at the equilibrium internuclear distance of the ion core $R_e^+ = 1.874$ Å, $[v^+ + 1]^{1/2}$ is the v dependence of the usual harmonic oscillator matrix element of the normal displacement coordinate and the final factor is the usual $n^{*-3/2}$ amplitude-in-the-core Rydberg scaling rule (Herzberg & Jungen 1972).

The intrachannel $\Delta v^+ = -1$ perturbations occur at n^* values where $\Delta G_{1/2} = \mathcal{R}[(n^* - n)^{-2} - (n^*)^{-2}]$, the vibrational spacing is equal to the electronic spacing. The n^* values for CaF, which has $\Delta G_{1/2} = 683\,\mathrm{cm}^{-1}$, occur as specified in table 9. The *only* core-penetrating state (Murphy *et al.* 1990) affected by an intrachannel perturbation in the $14 < n^* < 15$ region is the $0.55\ ^2\Sigma^+$ state! This state belongs to the Rydberg series that terminates (at low n^*) on the $X\ ^2\Sigma^+$ electronic ground state of CaF. This is a nominally sΣ series. Owing to the strongly penetrating, strongly shielding nature of the s series, the quantum defect derivative for this series is likely to be among the largest of all core-penetrating series. We have observed other examples of intrachannel $\Delta v^+ = -1$ perturbations in CaF (Murphy 1992), the largest of which is between $7.36\ ^2\Pi v = 0$ and $6.36\ ^2\Pi v = 1$ for which a perturbation matrix element of $21.9\,\mathrm{cm}^{-1}$ ($\mathrm{d}\mu/\mathrm{d}R = +0.732\,\mathrm{Å}^{-1}$) was observed (Gittins 1995). Using the Rydberg scaling law, and a crude estimate (C. M. Gittins, personal communication) of $\mathrm{d}\mu/\mathrm{d}R$ for the $0.55\ ^2\Sigma$ series of $0.18\,\mathrm{Å}^{-1}$, the perturbation matrix element for the $14.55\ ^2\Sigma^+ v^+ = 0$ state is estimated to be $\langle 14.55\ ^2\Sigma^+ v^+ = 0|\boldsymbol{H}'|9.55\ ^2\Sigma^+ v^+ = 1\rangle \approx 1.1\,\mathrm{cm}^{-1}$.

It is interesting to note that these intrachannel $\Delta v^+ = -1$ perturbations will be repeated, with minor modifications, for every value of v^+. The modifications are that, as v^+ increases, (i) the matrix elements increase as $(v^+)^{1/2}$, and (ii) $\Delta_{v+1/2}$ decreases, so the $N = 0$ energy gap between the $9.55\ ^2\Sigma^+ v^+ = 2$ perturber and the $14.55\ ^2\Sigma^+ v^+ = 1$ state is smaller than that between the corresponding $v^+ = 1$ perturber and $v^+ = 0$ state. The result is that, if an intrachannel perturbation occurs at finite N for $v^+ = 0$, it will be stronger and occur at lower N for $v^+ = 1$, etc., until the vibrational anharmonicity eventually shifts the perturbation to $N < 0$ and the effect of the intrachannel interaction begins to vanish.

R. N. Dixon (*School of Chemistry, University of Bristol, UK*). Dr Jungen's introduction to the history of molecular Rydberg spectroscopy implies that there was a long gap between the development of the basic theory for atoms and its application to molecules. Certainly, it was a long time before there was a good theoretical understanding of molecular Rydberg states. However, Dr Jungen's view was that of the theoretician and there were substantial experimental advances in the interim. Professor W. C. (Bill) Price, F.R.S. (1910–1993) must surely be considered to be the 'father' of experimental Rydberg spectroscopy and this discussion would not be complete without reference to his contribution.

In 1932, Bill Price went to Johns Hopkins University, Baltimore, on a Commonwealth Fund Fellowship, where he came under the influence of G. H. Dieke, A. H.

Pfund and R. W. Wood. Here he pioneered the techniques to study molecular spectroscopy in the vacuum ultraviolet ($\lambda < 200$ nm) and applied them to a wide range of molecules. His first great surprise was that the rich spectrum of acetylene bands between 105 and 152 nm could be interpreted in terms of the standard Rydberg quantum defect expression, and was the first to apply this to molecules. Professor R. S. Mulliken of Chicago quickly got in touch with him as soon as the first results were published—an interaction which lasted throughout their lives.

By 1936, Bill Price had published no fewer than 14 papers on molecular Rydberg spectroscopy, covering the molecules of O_2, C_2H_2, C_2H_4, HCN, CH_3I, C_2H_6, CH_3Br, CH_3Cl, H_2CO, alkyl alcohols, alkyl mercaptans, C_2H_5Br, C_2H_5Cl, C_2H_6 and C_2D_6. He had also published with Sydney Chapman a review article on the implications of this new spectroscopy for the understanding of the upper atmosphere. This research continued in Cambridge when Price returned to England and laid firm foundations for all the recent work in the field of this discussion.

Ch. Jungen. In my introduction (omitted in the printed version of the paper) I said that 'Balmer established his famous empirical formula describing the energy levels of the hydrogen atom in 1885. Only four years were to pass until 1889 when Rydberg was able to establish the modified formula which bears his name, thereby implicitly introducing the concept of the 'quantum defect'. As every physics student knows, Rydberg's discovery was based on the sodium atom in which he observed the s, p, d and f series of states. It took no less than 77 years before a correspondingly 'complete' system of Rydberg states was established in a molecule: in 1966 Miescher published an energy level diagram of the NO molecule and a list of corresponding quantum defects, which turned out to be quite similar to those known for the Na atom. The reason for this long delay is that, unlike in atoms, molecular Rydberg series are rarely directly observed as such. Rather they emerge from careful and extended fine structure analyses which take account of the nuclear degrees of freedom of the system studied, the molecular vibrations and rotations. As Miescher already recognized in his pioneering work on NO, the complications due to the presence of the nuclear degrees of freedom in molecular systems include the coupling of electronic and rotational-vibrational motions, in other words, the breakdown of the Born–Oppenheimer approximation, which disrupts the regularity of atom-like Rydberg structure as the ionization limit of a molecule is approached.' I think that because he based his work on detailed rotational analyses and took account of the breakdown of the Born–Oppenheimer approximation, Miescher went far beyond the scope of the earlier Rydberg spectroscopy. It is also fair to mention that Miescher carried out most of his experiments in the laboratories of the Canadian National Research Council in Ottawa where A. E. Douglas and G. Herzberg had initiated the construction of several new high-resolution spectrographs.

Additional references

Balmer, J. J. 1885 *Ann. D. Phys. Chem.* **25**, 80.

Gittins, C. M. 1995 Ph.D. thesis, MIT.

Herzberg, G. & Jungen, Ch. 1972 *J. Mol. Spectrosc.* **41**, 425.

Miescher, E. 1966 *J. Mol. Spectrosc.* **20**, 130.

Murphy, J. E. 1992 Ph.D. thesis, MIT.

Murphy, J. E., Berg, J. M., Merer, A. J., Harris, N. & Field, R. W. 1990 *Phys. Rev. Lett.* **65**, 1861.

Rydberg, J. R. 1890 *K. Svenska Vetenskaps Akad. Handlinger* **23**, 1.